ASTRONOMY & ASTROPHYSICS
SUPPLEMENT SERIES

Astron. Astrophys. Suppl. Ser. **103,** 5-32 (1994)

Hα velocity fields and rotation curves of galaxies in clusters*. II.

P. Amram[1], M. Marcelin[1], C. Balkowski[2], V. Cayatte[2], W.T. Sullivan III[3] and E. Le Coarer[1]

[1] Observatoire de Marseille, 2, place Le Verrier, 13248 Marseille Cedex 4, France
[2] Observatoire de Meudon, DAEC and URA 173, associé au CNRS et à l'Université Paris 7, 92195 Meudon Cedex, France
[3] Department of Astronomy, University of Washington, Seattle, WA 98195, U.S.A.

Received May 13; accepted June 1, 1993

Abstract. — Hα maps (continuum and line), velocity contour maps and rotation curves are presented for 15 galaxies in six different clusters: A 262, A 1367, Cancer, Coma (A 1656), Hercules (A 2151) and Pegasus I. These data have been obtained from two-dimensional Hα observations at the Canada-France-Hawaii Telescope equipped with PALILA, a scanning Pérot-Fabry interferometer. They complement the set of 21 galaxies already observed with the same instrumentation (Amram et al. 1992a).

Key words: galaxies: kinematics and dynamics — interferometry — clusters of galaxies — galaxies: ISM

1. Introduction

Various properties of galaxies in clusters are affected by environmental effects but their influence on the dynamics of galaxies has still to be clearly established. Such attempts have been made by Rubin et al. (1988), Whitmore et al. (1988) and Distefano et al. (1990), who suggested that the gradient of rotation curves is correlated with the distance of the galaxies from the cluster center, decreasing curves being found preferentially in the centers of clusters. Amram et al. (1993) do not confirm this result but this result must be established on a strong statistical basis, and it is therefore necessary to observe a large number of galaxies to be confident in the conclusions.

The aim of these series of observations is to increase our knowledge of the behaviour of galaxies in clusters in order to understand how their dynamics are affected by environmental effects. From an analysis of rotation curves of galaxies in clusters (Amram et al. 1992, hereafter called Paper I), we find no significant evidence for anything more than a small influence of the cluster environment on the dynamics of the individual galaxies (Amram et al. 1993).

The data for 15 galaxies presented in this paper follow those for a set of 21 galaxies already observed with the same instrumentation and published by the same authors in Paper I.

* based on observations obtained at the Canada-France-Hawaii Telescope

2. Observations

We have used the 3.6 cm CFH Telescope in Hawaii in October 1990 and March 1991, with the instrument PALILA attached at the Cassegrain focus. As for Paper I each galaxy was scanned in 24 steps through a Fabry-Pérot interferometer of interference order 1165 (free spectral range 257 km s^{-1}). The scanning steps were taken in two successive intercaled cycles to help minimizing biases due to changes in sky conditions during the total exposure. Only for the Hercules field (containing IC 1179, NGC 6050 and NGC 6054) did we expose for a single scanning cycle due to lack of time. The exposure time for each step varied from 180s to 420s so that the total exposure time per galaxy varied between 1^h12^m and 2^h48^m. The journal of the observations is given in Table I.

The CCD was the same Ford PHX1 as for the observations reported in Paper I, and was used in a binning mode giving an equivalent pixel of 1.14″ on the sky. The total field of view was $4.9' \times 4.9'$. Four extra galaxies were observed, but had insufficient Hα emission for a useful velocity field to be obtained. These galaxies are NGC 6022 (in Hercules), NGC 732, UGC 1344 and UGC 1350 (in A 262).

3. Data reduction

The details of the data reduction are given in Paper I. Let us recall the principles of observations with a scanning

Pérot-Fabry interferometer. For each galaxy observed we have a series of interference patterns obtained while scanning the interferometer (in this case 24 different images, each one obtained for a different step of the spacing between the plates of the interferometer). This enables to obtain, for each pixel of the observed galaxy, a detailed Hα profile within the free spectral range of the interferometer (in this case 5.6 Å, or 257 km s^{-1} at Hα rest wavelength).

3.1. *Velocity measurement*

Comparing the observed profile with the profile of a well known line produced by a calibration lamp (in that case the 6598.95 Å line of a Neon lamp) one can measure the Doppler-shift and thus deduce the radial velocity. An uncertainty remains, however, since the velocity is only known modulo the free spectral range.

This is easy to solve unambiguously knowing the redshift of the galaxy from slit spectroscopy or 21 cm - line observations. But another problem arises when the redshift of the galaxy brings its Hα emission line far from the calibration wavelength. In such a case a correction is required for dispersion in the multi-layer, semi-reflective coating on each interferometer plate; in other words, the effective optical spacing between the plates changes with wavelength.

This correction is theoretical in the present case and rapidly looses its accuracy when the redshifted Hα observed is far from the calibration wavelength. The Neon line used here is ideal for redshifts around 1000 to 2000 km s^{-1} but the correction becomes uncertain for redshifts higher than 10000 km s^{-1} (see below the remark about the systemic velocities of NGC 6050/I 1179 in the Comments on individual galaxies).

3.2. *Monochromatic and continuum images*

Since the interference pattern is produced only by the emission lines, it is possible to produce both pure Hα images and continuum images. For a given pixel the signal measured along the scanning sequence may be separated into two parts: (1) an almost constant level produced by the continuum light (typically over a bandpass of 20 Å), which is not affected by the scanning, and (2) a varying part produced by the monochromatic emission. The separation of these components is done by determining the continuum level above which we have monochromatic emission. More details are given in Paper I.

For each galaxy of our sample we give in Fig. 1 an optical photograph reproduced from the palomar Sky Survey prints, as well as the continuum and monochromatic images derived from the scanning sequence at Hα wavelength. Each image is accurate in its relative intensities, but our Pérot-Fabry technique does not allow an absolute calibration of intensities.

4. Velocity fields and rotation curves

The velocities measured for the Hα profile of each pixel enabled us to build detailed velocity fields for each galaxy, as explained in detail in Paper I. In order to improve the signal-to-noise ratio for the isovelocity contour plots displayed for each galaxy in Fig. 1, we have usually smoothed the original velocity field. The rotation curves of Fig. 1, however, have been derived from the original velocity points.

First estimates of the galaxy parameters necessary to derive each rotation curve were made from an analysis of the velocity field and the continuum image. The continuum gave estimates for the position of the nucleus as well as the inclination of the disk, and the isovelocity contours gave first estimates for position angle PA of the major axis, inclination, and systemic velocity.

These geometrical and kinematical parameters were then more precisely adjusted through an iterative process designed to minimize the dispersion of the velocity points about the rotation curve; in most cases this process did not change the parameters very much. The analysis utilized successive annuli in the plane of the galaxy corresponding to elliptical rings on the plane of the sky.

Our derived inclinations (see Table 2) are in good agreement with the values suggested by the axis ratio given in the RC3 catalogue of de Vaucouleurs et al. (1991), although on average our inclinations are higher by 3° compared to values deduced from the axis ratio (assuming a flat disk).

Our values of PA (see Table 2) are also generally within ±4° of those given in the RC3 catalogue. There are two exceptions: UGC 8161 for which our kinematic PA is close to that indicated by the outermost isophotes, while that given in RC3 matches the orientation of the inner disk. The other exception is IC 1179 (associated to and probably interacting with NGC 6050) for which there is a strong discrepancy since we find a PA of 158° while the value indicated in the RC3 is 36°. The RC3 value roughly matches the orientation of the bright central part of the galaxy but our value of PA is clearly indicated by the velocity field.

The rotation curves have been derived most often by taking into account all velocity points except those within 10° of the minor axis (except for two highly inclined galaxies: NGC 669 and UGC 8161, for which we excluded the points within 30° of the minor axis). Details of the method are given in Amram's (1991) thesis. The rotation curves for each galaxy are given in Fig. 1. The cloud of small points corresponds to all the individual rotation velocities measured within a ±30° sector centered on the major axis in the plane of the sky, no distinction being made between receding and approaching sides of the galaxy. Although these points represent only a portion of the pixels with measured velocities, they give a fair idea of the amount

and quality of our data. The velocity points with larger symbols are weighted means for the entire data set (±80° from the major axis in the sky plane) for the receding side (⊗) and the approaching side (⊙). The weights are proportional to cos θ, where θ is the angular separation of a pixel from the major axis as measured in the plane of the galaxy. The filled circles are then the weighted average of the approaching and receding sides, with error bars of ±1 rms for the mean of the velocity points within each annulus; those annuli with only one or two measured velocities have no error bars and are shown within parenthesis. These error bars are a measure of our overall random errors only in the case of well-behaved galaxies; effects such as internal absorption, non-circular motions, and warps can cause much greater additional uncertainties. The final rotation curve is a cubic spline function least-square fitted to these average points, weighted by their error. This fit is not very accurate in the very inner and outer portions of our galaxies, where we have few data. For the two galaxies already observed by Rubin et al. (1988) with a slit spectrograph (NGC 6054 and NGC 7591) we have also plotted their data using large squares of arbitrary size. For a fair comparison these data have been adjusted to our value of galaxy inclination. See Paper I, Sect. 6, for an earlier comparison with their slit spectroscopy. Finally, we note that the rotation velocity scale has not been multiplied by $(1+z)$, as should be done for an exact comparison with the amplitudes of rotation curves at other redshifts.

Table 2 summarizes parameters determined in the analysis: the systemic velocity $V_\odot$, the position angle of the major axis PA, and the inclination i, together with the corrected optical radius R_{25} ($= D_0/2$ in the RC3) at the 25$^{\rm th}$ magnitude per arcsec^2 isophote, the total corrected magnitude B_T°, and the morphological type of each galaxy (all from the RC3 catalogue of de Vaucouleurs et al. 1991). Note that according to the RC3 catalogue inclination correction to the diameters D_0 are no longer deemed to be justified.

Table 3 gives detailed information about the rotation curves. For each galaxy we give the following: Col. 1, the mean radius R (in arcseconds on the major axis) of the annulus for which the rotational velocity is calculated; Col. 2, the number of points $N_{\rm app}$ with measurable radial velocities in this annulus for the approaching side of the galaxy; Col. 3, the weighted average velocity $V_{\rm app}$ calculated from these velocity points; Col. 4, the error $e_{\rm app}$ in the mean velocity $V_{\rm app}$ (±1 rms); Cols. 5, 6 and 7, similar to Cols. 2, 3 and 4, but for the receding side ($N_{\rm rec}, V_{\rm rec}$ and $e_{\rm rec}$); Col. 8, the total number N of velocity points in the annulus ($N = N_{\rm app} + N_{\rm rec}$); Col. 9, the average velocity V computed from both sides; and Col. 10, the corresponding error e (±1 rms) in this mean velocity (as displayed by the error bars in the plotted rotation curves of Fig. 1).

5. Comments on clusters and individual galaxies

Cluster A262: The cluster A262 is one of the most conspicuous condensations in the Pisces-Perseus supercluster. It has been extensively studied in X-rays and in the radio continuum. It is a spiral-rich cluster, characterized by the presence of a central X-ray source centered on a D galaxy. These characteristics recall those of the Virgo cluster. Giovanelli et al. (1982) have studied the HI content of the spiral galaxies and shown that some of them are HI-deficient. We have chosen to observe deficient and non deficient galaxies at different distance from the centre of the cluster. Three of these galaxies were not detected in Hα (NGC 732, UGC 1344 and UGC 1350).

NGC 668: The continuum isophotes to the South must be considered with care because parasitic light affecting this exposure can be only very roughly subtracted.

Although the Hα emission is much brighter and more extended toward the South, the rotation curve is fairly symmetric and can be followed as far to the north as to the south.

NGC 669: This galaxy was noticed by Giovanelli et al. (1982) to have the largest optical linear diameter in the cluster and to be one of the brightest object in the field. However its most remarkable characteristic is the enormous width of its HI profile and its HI deficiency.

Several interfering reflections (out of focus) of field stars, occurring between the plates of the interferometer and the interference filter, can be seen on the edges of the continuum image.

The Hα emission is very faint and lost in the noise background. Because of the faint S/N ratio, we have only been able to indicate average values of the plateaus of the rotation curve when drawing the velocity field. The dispersion on the measured radial velocities is high. It extends almost twice as far out for the approaching side, which has weaker Hα emission.

N.B.: Let us recall that the velocities measured with our fabry-Perot are determined modulo 263 km s^{-1} for this galaxy. The high inclination, added to the faint S/N ratio, prevents applying the usual method in which one follows the velocity gradient along the major axis and add or subtract one free spectral range whenever a discontinuity is observed. The positions of the peaks of the HI profile from Giovanelli et al. 1982 bring poor help in this case since two solutions appear equally probable: Northern plateau at 5000 km s^{-1} with Southern plateau at 4480 km s^{-1} or Northern plateau at 4474 km s^{-1} and Southern plateau at 5006 km s^{-1}. We choose the first solution because our interference filter favours the higher velocities and that the observed Hα emission is, in average, brighter to the North (see monochromatic image). However the second solution is not excluded.

NGC 688: The rotation curve exhibits a marked bump at $30'' - 50''$ from the center, coinciding approximately with the end of the galaxy's bar. This reminds of the case of NGC 5383 (Duval & Athanassoula 1983). Furthermore one can see that the isovelocity lines are tilted within the bar so that their orientation approaches that of the bar major axis, and that the systemic velocity contour has the classical Z shape observed in most barred galaxies (see Amram et al. 1992b).

UGC 1347: A prominent field star is close to the galaxy, on its SE edge. Another seemingly stellar object can be seen to the South on our continuum isophotes but nothing is found at that place on the PSS photograph. Recent deep CCD exposures taken in R and B bands by G. Comte at the Pic du Midi 2 m telescope (in November 1992) do not show any object at that place. According to Brian Marsden (private communication) there was no minor planet or comet in the vicinity at the date we observed. There was also no known supernova or known or suspected variable star of any type.

NGC 753: This galaxy is relatively close to the cluster center but it is not HI-deficient (Giovanelli et al. 1982). The extension of the continuum isophotes to the North of the galaxy is merely due to a spurious reflection (out of focus) of the bright nucleus. It has, however, no influence on the Hα image or the measured velocities. The outer SW arm exhibits an anomalous behaviour where the isovelocity lines change orientation suddenly toward the South when crossing this arm. In order to save symmetry the velocity points measured inside this arm have been excluded from the plot of the rotation curve. If they were included the curve for the receding side would rise strongly at its end. The simplest explanation is that this outer arm does not lie in the plane of the disk. Whereas an inclination of 50° is found for the galaxy as a whole, a clearly smaller value (around 30°) is found for this arm.

UGC 1493: Although very distant from the center of the cluster A262 to which this galaxy belongs, UGC 1493 is very HI-deficient (Giovanelli et al. 1982). The extension of the continuum isophotes to the North is merely the spurious reflection of the bright star seen to the South of the galaxy; it has no influence on the Hα image nor on our measured velocities.

Cancer cluster

Z 119-051: The Hα image shows a spiral structure unexpected from the appearance of the continuum image. The shape of the rotation curve, gently rising all along the optical disk, is similar to that already observed in Paper I for 4 of 5 galaxies from the Zwicky catalogue; these tend to be late-type galaxies of high surface brightness.

A1367 cluster

NGC 3861: The continuum isophotes on the Northern edge of the image are produced by a spurious reflection of the bright nucleus of the galaxy. A close companion to the SE is clearly seen on the continuum map. Its Hα emission is faint, and we have omitted its poorly determined velocity points from the plotted velocity field.

The rotation curve exhibits a pronounced local maximum between $30''$ and $35''$ from the center, coinciding with the outer part of a seemingly annular structure visible on the Hα image and PSS photograph.

NGC 3883: This galaxy has an anemic appearance (as defined by van den Bergh 1976) it is also very red although very HI rich (Schommer & Bothun, 1983). It has been mapped in HI by van der Hulst et al. (1987).

The Hα emission is very patchy. As a consequence the velocity field exhibits a large number of uncertain (dashed) isovelocity lines. Nevertheless the rotation curve is well defined for radii $> 25''$; no Hα could be detected inside this radius.

This galaxy exhibits a clear warp (see the continuum isophotes of Fig. 1) with PA = 45° for the isophotes of the inner disk and PA = 53° for the outermost isophotes. The latter value was adopted for our rotation curve in order to minimize the dispersion in the outer part.

Coma cluster

UGC 8161: The weak, scattered Hα emission makes the velocity field uncertain. Because of the galaxy's high inclination, the rotation curve has been derived from the velocity points within 60° of the major axis instead of the usual 80°.

Hercules cluster

IC 1179/NGC 6050: These two galaxies were observed serendipitously together with NGC 6054. This pair is also known as Arp 272; NGC 6050 is to the NE of IC 1179.

Our continuum isophotes are strongly biased because the galaxies were on the very edge of the interference filter. To make things worse, a spurious reflection from a bright nearby field galaxy (IC 1182) contaminates the outermost isophotes to the North of NGC 6050. We therefore chose to draw the continuum isophotes with a rather high threshold to show both galaxies clearly separated and two bright spots visible for IC 1179. Although IC 1179 appears clearly more extended than its companion in Hα emission, this is due to its redshift matching better our interference filter. IC 1179 has its Hα redshifted to 6804 Å whereas NGC 6050 is redshifted only to 6770 Å, thus falling well outside the main portion of the passband of the interference filter.

Note the strong continuum spot to the NW of N 6050, which may be a small elliptical companion since it has no Hα emission at all.

The two velocity fields could be drawn rather easily, even for NGC 6050 despite the faint transmission at its velocity. NGC 6050 exhibits a regular spiral structure and velocity field, but IC 1179 exhibits a distorted structure and velocity field. Nevertheless both rotation curves appear quite acceptable. We hardly reach 0.8 R_{25} for NGC 6050 but reach almost to 2 R_{25} in the case of IC 1179, especially because of the approaching side extending twice as far as the receding side.

For these galaxies and NGC 6054 (which is in the same field) we had a special problem determining the systemic velocity. For such high redshifts the Hα wavelength is far from the adopted calibration wavelength (a Neon line at 6598.95 Å) and the phase correction applied to the velocities becomes less precise, especially since it is computed for a theoretical coating of the interferometer plates. Comparing with published radio redshifts (RC3 for NGC 6054, Freudling et al. 1992 for NGC 6050 and IC 1179) it appears that our velocities are systematically low by 150 km s^{-1} (-155 km s^{-1} for IC 1179, -159 km s^{-1} for NGC 6050 and -107 km s^{-1} for NGC 6054). We have however, not applied any correction.

NGC 6054: The Hα emission is rather faint and only clearly visible in the bar where it is strongly asymmetric, being much more extended toward the North. The S/N ratio is poor since the exposure was limited to 1h12mn. The outermost isophotes have been drawn at the limit of the sky background for the continuum image as well as the Hα image, but still very little emission can be seen outside the bar. The rotation curve is fairly symmetric despite the large dispersion. The geometrical parameters are not easy to determine accurately because the S/N ratio is low. For purposes of comparison we have therefore decided to adopt the same values as Rubin et al.'s (1988). Our rotation curve agrees with theirs (big squares) within the errors.

Pegasus I cluster

NGC 7591: This galaxy has also been observed by Rubin et al. (1988). Their rotation curve (plotted with big squares) is in good agreement with our curve although the "waves" of the two curves seem out of phase.

J 2318+0633: This anonymous galaxy (not in the RC3 catalogue and named here according to its 2000 coordinates) is in the same field of view as NGC 7591.

The strange behaviour of the isophotes of the bright star to the SE is due to its location on the edge of the field.

The fact that the Hα emission of J 2318+0633 shows up through the same interference filter as NGC 7591 suggests that it has a similar velocity and belongs to the Pegasus cluster. However, with a Pérot-Fabry interferometer the velocity may only be determined modulo the free spectral range ($n \times 261$ km s^{-1}) the value of $V_S = 5008$ km s^{-1} is rather arbitrarily chosen in Table 2. The rotation curve is of course unaffected.

Because no value of R_{25} is available from the literature for this galaxy, we have estimated it as $20'' \pm 5''$ by comparison with the continuum image of NGC 7591 since they were observed together in the same field of view.

The outermost isophotes drawn when measuring the R_{25} suggest a PA of around 135° while our analysis of the velocity field indicates 173° (see Table 2). In fact this galaxy is certainly strongly warped; the isophotes of the continuum image of Fig. 1 show that the inner disk exhibits a PA close to 180° while the outer isophotes show a PA progressively shifting to 160°.

6. Summary

Hα maps (continuum and line), velocity fields and rotation curves of 15 galaxies in 6 different clusters have been presented.

This new sample supplements a first sample of 21 galaxies (Paper I) for which we found no correlation between the gradients of the rotation curves and the location of the galaxies in the clusters (Amram et al. 1993). A detailed analysis of the complete sample will appear in a forthcoming paper, but a preliminary analysis (Amram et al. 1991) also shows little, if any, correlation.

Acknowledgements. We thank the entire CFHT staff, and more especially Guy Monnet and Berndt Grundseth, for their help at the 3.6 m CFH Telescope. We are indebted to Jacques Boulesteix for his help with reducing the data using his software packages VISU 2 and VISU 3. We also thank G. Comte for having taken a CCD exposure of UGC 1347 at Pic du Midi Observatory. WTS thanks the American Astronomical Society for its support through a Small Research Grant and the NATO International Scientific Exchange Programme for a Collaborative Research Grant. This work has been supported by the Groupement de Recherche "Cosmologie", and by the Ministry of Education through a DAGIC program allocated to the Paris 7 University.

References

Amram P. 1991, Thesis, Université de Provence (Aix-Marseille I)

Amram P., Balkowski C., Cayatte V., Le Coarer E., Marcelin M., Sullivan W.T. 1991, Proceedings of the NATO Workshop on Clusters (July 1991) Cambridge, in press

Amram P., Le Coarer E., Marcelin M., Balkowski C., Sullivan W.T., Cayatte V. 1992a, A&AS 94, 175

Amram P., Marcelin M., Bonnarel F., Boulesteix J., Afanasiev V.L., Dodonov S.N. 1992b, A&A 263, 69

Amram P., Sullivan W.T., Balkowski C., Marcelin M., Cayatte V. 1993, ApJ 403, L59

Arp H. 1966, Atlas of peculiar galaxies, Carnegie Institution of Washington

De Vaucouleurs G., De Vaucouleurs A., Corwin H.G.Jr, Buta R., Paturel G., Fouqué P. 1991, Third Reference Catalogue of Bright Galaxies, (RC3), ed. Springer Verlag

Distefano A., Rampazzo R., Chincarini G., de Souza R. 1990, A&AS 86, 7

Duval M.F., Athanassoula E. 1983, A&A 121, 297

Freudling W., Haynes M.P., Giovanelli R. 1992, ApJS 79, 157

Giovanelli R., Haynes M.P., Chincarini G. 1982, ApJ 262, 442

Rubin V.C., Whitmore B.C., Ford W.K. 1988, ApJ 333, 522

Schommer R.A., Bothun G.D. 1983, AJ 88, 577

van den Bergh S. 1976, ApJ 206, 883

van der Hulst J.M., Skillman E.D., Kennicut R.C., Bothun G.D. 1987, A&A 177, 63

Whitmore B.C., Forbes D.A., Rubin V.C. 1988, ApJ 333, 542

Table 1. Log of the observations

Name of galaxy	Coordinates (1950) (RC3) α	δ	Total exposure time	Observation date	Interference filter (central wavelength λ_o and FWHM)
ABELL 262 CLUSTER					
NGC 668	$1^h43^m27^s$	36°12'40"	1^h52^m	October 25 1990	6655Å,20Å
NGC 669	$1^h44^m21^s$	35°18'51"	2^h48^m	October 26 1990	6670Å,20Å
NGC 688	$1^h47^m49^s$	35°02'13"	1^h52^m	October 25 1990	6655Å,20Å
UGC 1347	$1^h49^m49^s$	36°22'21"	2^h48^m	October 25 1990	6690Å,22Å
NGC 753	$1^h54^m45^s$	35°40'22"	2^h24^m	October 26 1990	6670Å,20Å
UGC 1493	$1^h57^m55^s$	37°58'13"	2^h24^m	October 27 1990	6655Å,20Å
CANCER CLUSTER					
Z 119-051	$8^h16^m24^s$	20°55'	1^h52^m	March 21 1991	6670Å,20Å
ABELL 1367 CLUSTER					
NGC 3861	$11^h42^m29^s$	20°15'05"	1^h52^m	March 20 1991	6712Å,10Å
NGC 3883	$11^h44^m12^s$	20°57'16"	1^h52^m	March 21 1991	6720Å,50Å
COMA CLUSTER					
UGC 8161	$13^h01^m04^s$	26°49'06"	1^h52^m	March 21 1991	6712Å,10Å
HERCULES CLUSTER					
IC 1179	$16^h03^m07^s$	17°53'15"	1^h12^m	March 20 1991	6799Å,16Å
NGC 6050	$16^h03^m09^s$	17°53'37"	1^h12^m	March 20 1991	6799Å,16Å
NGC 6054	$16^h03^m16^s$	17°54'13"	1^h12^m	March 20 1991	6799Å,16Å
PEGASUS I CLUSTER					
NGC 7591	$23^h15^m44^s$	6°18'45"	2^h48^m	October 27 1990	6670Å,20Å
J 2318+0633	$23^h15^m52^s$*	6°16'36"*	2^h48^m	Octobre 27 1990	6670Å,20Å

* Coordinates 2000 are $\alpha = 23^h18^m24^s$ $\delta = 6°33'$, adopted for the name of the galaxy

Table 2. Galaxy parameters

Name of galaxy	$R25_{corrected}$ (")	B_T°	T	$V_\odot$ (km s^{-1})	PA (°)	i (°)
ABELL 262 CLUSTER						
NGC 668	55.9	13.1	3	4497	33	50
NGC 669	97.1	13.0	2	4740	39	80
NGC 688	75.4	12.7	3	4118	146	55
UGC 1347	39.5	13.4	5	5478	18	30
NGC 753	78.9	12.3	4	4855	128	50
UGC 1493	57.2	13.2	2	4143	85	65
CANCER CLUSTER						
Z 119-051	16.4			4985	138	50
ABELL 1367 CLUSTER						
NGC 3861	68.7	13.1		5075	73	60
NGC 3883	88.5	13.2	3	6942	161	35
COMA CLUSTER						
UGC 8161	32.2	14.6		6665	146	70
HERCULES CLUSTER						
IC 1179	17.7	15.7	6	10973*	158	50
NGC 6050	26.1	15.0	5	9430*	125	50
NGC 6054	20.8	15.4	3	11083*	176	60
PEGASUS I CLUSTER						
NGC 7591	59.9	13.0	4	4890	143	65
J 2318+0633	20±5**			5008±nx261**	173	60

* Systemic velocities contain a systematic error of ~ 150 km s^{-1}; see the comments for IC 1179/NGC 6050
** See comments for J 2318 + 0633

Table 3.

R (1)	N_app (2)	V_app (3)	e_app (4)	N_rec (5)	V_rec (6)	e_rec (7)	N (8)	V (9)	e (10)
Cluster : A262 - Galaxy : NGC 668									
R	N_app	V_app	e_app	N_rec	V_rec	e_rec	N	V	e
1.0	1	95 ± 0		3	75 ± 31		4	81 ± 26	
3.0	9	139 ± 32		6	146 ± 30		15	142 ± 30	
5.0	13	183 ± 12		13	180 ± 33		26	181 ± 24	
7.0	21	194 ± 24		20	187 ± 25		40	191 ± 21	
9.0	27	202 ± 15		27	193 ± 23		54	197 ± 20	
11.0	31	192 ± 20		31	189 ± 20		62	190 ± 20	
13.0	36	183 ± 13		33	194 ± 22		69	188 ± 18	
15.0	48	182 ± 8		41	194 ± 22		89	188 ± 17	
17.0	47	187 ± 13		30	184 ± 22		77	186 ± 17	
19.0	54	189 ± 14		29	193 ± 35		83	190 ± 22	
21.0	52	184 ± 18		34	193 ± 32		86	187 ± 24	
23.0	60	182 ± 17		33	205 ± 47		93	189 ± 31	
25.0	47	181 ± 19		21	188 ± 48		68	183 ± 29	
27.0	47	187 ± 31		23	167 ± 46		70	181 ± 37	
29.0	41	183 ± 26		14	166 ± 40		55	178 ± 31	
31.0	48	181 ± 16		11	168 ± 46		59	179 ± 23	
33.0	43	178 ± 22		19	180 ± 36		62	179 ± 26	
35.0	42	185 ± 17		17	175 ± 43		59	182 ± 25	
37.0	58	187 ± 13		24	185 ± 31		82	186 ± 19	
39.0	30	191 ± 16		16	179 ± 36		46	188 ± 22	
41.0	21	180 ± 23		20	173 ± 47		41	178 ± 33	
43.0	18	171 ± 26		9	229 ± 66		27	184 ± 44	
45.0	16	174 ± 25		10	202 ± 51		26	184 ± 38	
47.0	12	174 ± 28		20	190 ± 34		32	184 ± 32	
49.0	8	170 ± 24		10	185 ± 20		18	178 ± 22	
51.0	10	166 ± 31		2	192 ± 18		12	171 ± 30	
53.0	7	184 ± 24		0			7	184 ± 24	
55.0	9	182 ± 15		0			9	182 ± 15	
57.0	5	191 ± 3		0			5	191 ± 3	
Cluster : A262 - Galaxy : NGC 669									
R	N_app	V_app	e_app	N_rec	V_rec	e_rec	N	V	e
4.0	1	148 ± 0		2	299 ± 63		3	247 ± 99	
12.0	6	291 ± 74		4	375 ± 74		10	325 ± 82	
20.0	7	385 ± 54		3	353 ± 131		10	375 ± 78	
28.0	10	382 ± 54		9	251 ± 83		19	314 ± 96	
36.0	19	276 ± 100		19	255 ± 41		38	265 ± 75	
44.0	16	292 ± 95		12	326 ± 99		28	305 ± 96	
52.0	6	189 ± 76		25	320 ± 69		31	293 ± 87	
60.0	9	278 ± 7		25	277 ± 48		34	277 ± 41	
68.0	19	354 ± 56		4	301 ± 46		23	344 ± 57	
76.0	12	326 ± 53		2	378 ± 20		14	333 ± 53	
84.0	12	312 ± 20		0			12	312 ± 20	
92.0	16	309 ± 52		0			16	309 ± 52	
100.0	9	343 ± 51		0			9	343 ± 51	
108.0	7	337 ± 61		0			7	337 ± 61	
116.0	2	318 ± 1		0			2	318 ± 1	
124.0	2	349 ± 1		0			2	349 ± 1	
132.0	3	425 ± 59		0			3	425 ± 59	
140.0	1	387 ± 0		0			1	387 ± 0	
148.0	1	403 ± 0		0			1	403 ± 0	

Table 3. continued

Cluster : A262 - Galaxy : NGC 688

R	N_app	V_app	e_app	N_rec	V_rec	e_rec	N	V	e
7.5	7	108	± 56	2	92	± 46	9	106	± 53
10.5	22	128	± 34	19	130	± 22	41	129	± 28
13.5	33	157	± 27	37	159	± 22	70	158	± 24
16.5	46	168	± 17	50	186	± 13	96	177	± 17
19.5	47	190	± 15	44	198	± 11	91	194	± 13
22.5	45	207	± 15	30	207	± 5	75	207	± 12
25.5	36	217	± 13	19	210	± 9	55	214	± 12
28.5	26	214	± 21	15	224	± 12	41	218	± 19
31.5	26	207	± 19	5	218	± 9	31	208	± 18
34.5	14	215	± 21	8	224	± 13	22	218	± 18
37.5	13	221	± 16	20	228	± 29	33	225	± 25
40.5	14	219	± 22	16	226	± 20	30	223	± 20
43.5	15	203	± 33	12	205	± 36	27	204	± 34
46.5	37	191	± 32	32	174	± 30	69	184	± 32
49.5	76	184	± 27	35	180	± 41	110	183	± 31
52.5	65	194	± 27	16	209	± 50	81	196	± 32
55.5	38	215	± 27	31	207	± 39	69	211	± 33
58.5	35	219	± 13	41	199	± 29	76	209	± 24
61.5	19	218	± 10	31	195	± 47	50	206	± 37
64.5	4	255	± 22	10	235	± 29	14	244	± 27
67.5	2	272	± 4	1	248	± 0	3	266	± 13

Cluster : A262 - Galaxy : UGC 1347

R	N_app	V_app	e_app	N_rec	V_rec	e_rec	N	V	e
1.5	0			4	26	± 10	4	26	± 10
4.5	11	67	± 20	12	61	± 17	23	63	± 18
7.5	29	78	± 16	27	75	± 9	56	76	± 13
10.5	55	93	± 11	47	83	± 13	102	88	± 13
13.5	63	96	± 11	46	95	± 21	109	95	± 16
16.5	77	91	± 14	60	112	± 20	136	100	± 19
19.5	104	98	± 14	71	109	± 20	175	102	± 18
22.5	97	101	± 11	71	105	± 19	168	102	± 15
25.5	84	101	± 15	62	105	± 15	146	103	± 15
28.5	42	105	± 23	69	101	± 19	111	102	± 20
31.5	22	108	± 27	42	103	± 20	64	104	± 22
34.5	10	107	± 19	24	101	± 10	34	102	± 13

Cluster : A262 - Galaxy : NGC 753

R	N_app	V_app	e_app	N_rec	V_rec	e_rec	N	V	e
2.5	13	104	± 25	11	88	± 33	24	97	± 29
7.5	50	151	± 18	46	180	± 29	96	165	± 28
12.5	81	189	± 22	80	197	± 25	161	193	± 24
17.5	90	179	± 22	101	192	± 25	191	186	± 25
22.5	145	191	± 15	131	210	± 26	276	201	± 23
27.5	168	198	± 18	154	221	± 18	322	209	± 21
32.5	198	205	± 18	93	226	± 27	291	211	± 23
37.5	161	205	± 27	68	205	± 33	229	205	± 29
42.5	119	201	± 29	117	204	± 23	236	203	± 27
47.5	102	204	± 28	104	198	± 23	206	201	± 26
52.5	132	206	± 29	120	199	± 20	252	203	± 25
57.5	127	219	± 29	117	190	± 14	244	203	± 26
62.5	90	215	± 37	81	184	± 14	171	197	± 30
67.5	71	190	± 33	64	193	± 15	135	192	± 24
72.5	77	195	± 16	46	189	± 25	123	193	± 20
77.5	95	204	± 17	57	229	± 37	152	210	± 27
82.5	48	215	± 20	67	255	± 25	115	231	± 29
87.5	18	206	± 17	8	245	± 35	26	211	± 24

Table 3. continued

Cluster : A262 - Galaxy : UGC 1493

R	N_app	V_app	e_app	N_rec	V_rec	e_rec	N	V	e
1.5	5	82	± 15	4	127	± 28	9	101	± 31
4.5	14	134	± 21	14	139	± 39	28	137	± 31
7.5	19	156	± 11	19	151	± 30	38	154	± 22
10.5	33	169	± 16	33	159	± 15	66	164	± 16
13.5	38	186	± 13	38	169	± 17	76	177	± 18
16.5	52	188	± 22	51	169	± 25	102	179	± 25
19.5	54	189	± 23	56	172	± 21	110	181	± 24
22.5	56	189	± 21	64	172	± 17	119	181	± 19
25.5	63	189	± 24	74	174	± 16	137	181	± 22
28.5	46	187	± 21	76	179	± 15	122	182	± 18
31.5	19	173	± 19	52	187	± 22	71	182	± 22
34.5	17	164	± 12	17	191	± 25	34	176	± 23
37.5	15	165	± 6	11	188	± 23	26	173	± 18
40.5	0			7	194	± 7	7	194	± 7
43.5	0			7	178	± 14	7	178	± 14
46.5	0			2	176	± 1	2	176	± 1

Cluster : Cancer - Galaxy : Z119-051

R	N_app	V_app	e_app	N_rec	V_rec	e_rec	N	V	e
1.0	1	15	± 0	2	48	± 8	3	40	± 19
3.0	3	50	± 10	4	81	± 41	7	66	± 32
5.0	6	71	± 16	10	71	± 22	16	71	± 19
7.0	12	79	± 21	12	73	± 18	24	76	± 19
9.0	12	83	± 40	18	74	± 14	30	78	± 28
11.0	11	80	± 34	14	79	± 12	25	79	± 24
13.0	12	107	± 28	18	93	± 18	30	99	± 24
15.0	13	129	± 25	21	103	± 18	34	114	± 25
17.0	15	124	± 16	20	114	± 13	35	118	± 15
19.0	20	118	± 19	14	111	± 30	34	116	± 23
21.0	5	113	± 19	10	124	± 13	15	121	± 15
23.0	0			3	107	± 9	3	107	± 9

Cluster : A1367 - Galaxy : NGC 3861-UGC 672

R	N_app	V_app	e_app	N_rec	V_rec	e_rec	N	V	e
7.5	0			3	279	± 23	3	279	± 23
10.5	0			7	310	± 51	7	310	± 51
13.5	1	343	± 0	11	283	± 36	12	286	± 38
16.5	11	218	± 109	8	279	± 18	19	251	± 80
19.5	12	243	± 94	23	246	± 46	35	245	± 62
22.5	35	277	± 25	26	253	± 35	61	267	± 31
25.5	30	297	± 35	25	265	± 58	55	284	± 48
28.5	28	312	± 34	20	281	± 50	48	298	± 44
31.5	20	300	± 45	16	310	± 34	36	304	± 40
34.5	19	308	± 50	15	309	± 33	34	308	± 44
37.5	12	289	± 37	15	298	± 34	27	294	± 34
40.5	21	273	± 34	7	289	± 56	28	278	± 42
43.5	20	269	± 25	25	252	± 69	45	257	± 60
46.5	20	275	± 20	35	231	± 59	55	245	± 54
49.5	37	263	± 17	19	249	± 26	56	259	± 21
52.5	45	268	± 20	21	255	± 43	66	265	± 28
55.5	35	269	± 38	15	235	± 17	50	260	± 37
58.5	33	263	± 36	16	264	± 30	49	263	± 34
61.5	26	254	± 31	5	328	± 27	31	264	± 40
64.5	9	268	± 28	5	288	± 85	14	277	± 56
67.5	0			4	220	± 14	4	220	± 14

Table 3. continued

Cluster : A1367 - Galaxy : NGC 3883

R	N_app	V_app	e_app	N_rec	V_rec	e_rec	N	V	e
26.0	37	176	18	15	162	12	52	170	17
30.0	58	183	18	12	156	5	70	176	19
34.0	35	151	35	38	167	15	73	161	26
38.0	44	152	27	74	172	17	118	168	21
42.0	36	180	35	30	183	22	66	182	28
46.0	13	139	18	25	174	9	38	169	17
50.0	16	180	22	10	166	6	26	170	15
54.0	20	163	31	45	177	14	65	175	19
58.0	44	163	17	91	172	15	135	170	16
62.0	40	168	13	36	162	8	76	164	11
66.0	19	170	15	24	154	7	43	160	13
70.0	22	171	12	7	173	10	29	171	12
74.0	23	163	15	6	158	12	29	162	14
78.0	11	172	10	40	154	12	51	157	13
82.0	19	163	20	55	156	16	74	157	17
86.0	11	137	19	16	161	11	27	153	18
90.0	23	149	17	0			23	149	17
94.0	9	158	18	0			9	158	18
98.0	6	176	8	0			6	176	8

Cluster : Coma - Galaxy : UGC 8161

R	N_app	V_app	e_app	N_rec	V_rec	e_rec	N	V	e
1.5	2	50	11	1	21	0	3	42	19
4.5	2	71	27	0			2	71	27
13.5	0			12	80	16	12	80	16
16.5	0			14	88	18	14	88	18
19.5	3	92	16	9	98	20	12	96	18
22.5	14	83	12	6	101	11	20	88	14
25.5	19	86	11	8	95	8	27	88	11
28.5	14	103	9	2	99	12	16	103	9
31.5	2	85	5	0			2	85	5
34.5	1	87	0	1	112	0	2	106	18
37.5	0			10	103	6	10	103	6
40.5	0			6	103	8	6	103	8

Cluster : Hercules - Galaxy : I1179

R	N_app	V_app	e_app	N_rec	V_rec	e_rec	N	V	e
1.0	2	30	11	2	17	12	4	23	12
3.0	7	50	36	7	45	37	13	50	33
5.0	4	114	30	8	81	46	12	91	43
7.0	7	116	36	15	102	28	22	106	31
9.0	13	120	20	17	103	27	30	110	25
11.0	20	112	25	10	128	58	30	117	38
13.0	27	114	14	8	128	46	35	117	25
15.0	33	123	21	9	134	27	42	126	22
17.0	23	130	26	3	154	32	26	134	28
19.0	14	134	13	0			14	134	13
21.0	15	130	6	0			15	130	6
23.0	14	133	38	0			14	133	38
25.0	10	151	48	0			10	151	48
27.0	5	139	21	0			5	139	21
29.0	2	126	11	0			2	126	11
31.0	7	146	32	0			7	146	32
33.0	5	149	26	0			5	149	26

Table 3. continued

Cluster : Hercules - Galaxy : NGC 6050

R	N_app	V_app	e_app	N_rec	V_rec	e_rec	N	V	e
1.5	0			1	116	± 0	1	116	± 0
4.5	3	232	± 74	9	145	± 26	12	164	± 52
7.5	25	179	± 41	32	174	± 29	57	176	± 35
10.5	25	192	± 40	36	189	± 33	61	190	± 36
13.5	15	216	± 28	29	199	± 37	44	206	± 34
16.5	11	176	± 30	20	179	± 35	31	178	± 34
19.5	8	155	± 16	10	207	± 15	18	187	± 30

Cluster : Hercules - Galaxy : NGC 6054

R	N_app	V_app	e_app	N_rec	V_rec	e_rec	N	V	e
1.5	6	101	± 37	2	75	± 7	7	95	± 35
4.5	14	133	± 28	3	122	± 27	17	131	± 27
7.5	19	133	± 27	10	123	± 34	29	130	± 29
10.5	10	142	± 24	19	150	± 42	29	148	± 37
13.5	10	175	± 23	7	159	± 23	17	166	± 24
16.5	19	155	± 53	8	153	± 31	27	154	± 45
19.5	31	126	± 41	16	124	± 27	47	125	± 36
22.5	20	121	± 47	9	120	± 48	29	121	± 46
25.5	10	173	± 27	1	220	± 0	11	175	± 28

Cluster : Pegasus - Galaxy : NGC 7591

R	N_app	V_app	e_app	N_rec	V_rec	e_rec	N	V	e
2.0	6	253	± 68	7	308	± 32	12	279	± 59
6.0	19	255	± 47	19	252	± 61	38	253	± 54
10.0	29	217	± 63	31	231	± 45	60	224	± 54
14.0	35	226	± 36	37	226	± 46	72	226	± 41
18.0	42	222	± 40	34	235	± 34	76	228	± 38
22.0	42	238	± 55	36	244	± 36	78	241	± 46
26.0	43	224	± 34	46	239	± 43	89	232	± 39
30.0	62	210	± 38	80	231	± 35	141	222	± 37
34.0	73	204	± 33	85	209	± 42	158	207	± 38
38.0	79	218	± 25	83	205	± 38	162	211	± 34
42.0	70	218	± 32	96	207	± 36	166	211	± 35
46.0	65	214	± 25	71	201	± 40	136	208	± 33
50.0	52	207	± 19	50	218	± 43	102	211	± 31
54.0	24	224	± 28	23	207	± 50	47	217	± 39
58.0	27	225	± 29	16	223	± 49	43	224	± 37
62.0	24	239	± 31	20	225	± 26	44	232	± 29
66.0	27	222	± 36	12	209	± 23	39	218	± 33
70.0	13	213	± 22	4	229	± 27	17	216	± 23
74.0	19	209	± 23	14	210	± 20	33	209	± 21
78.0	1	249	± 0	27	211	± 26	28	212	± 27
82.0	0			47	217	± 34	47	217	± 34
86.0	0			18	215	± 41	18	215	± 41
94.0	0			6	220	± 47	6	220	± 47

Table 3. continued

Cluster : Pegasus - Galaxy : 2318+0633

R	N_app	V_app	e_app	N_rec	V_rec	e_rec	N	V	e
1.5	1	33	0	2	37	26	3	35	18
2.5	4	64	27	3	82	11	7	73	22
3.5	2	91	9	2	97	3	4	94	7
4.5	5	86	23	1	113	0	6	92	23
5.5	6	129	38	5	119	22	11	124	30
6.5	4	142	22	4	140	11	8	141	16
7.5	5	150	24	4	139	11	9	144	19
8.5	4	156	33	8	141	14	12	146	22
9.5	3	159	32	5	136	17	8	144	24
10.5	3	152	21	9	139	21	12	142	21
11.5	1	126	0	3	147	15	4	141	16
12.5	2	138	6	5	157	35	7	150	28
13.5	1	150	0	3	156	18	4	155	15
14.5	1	148	0	3	155	14	4	153	11

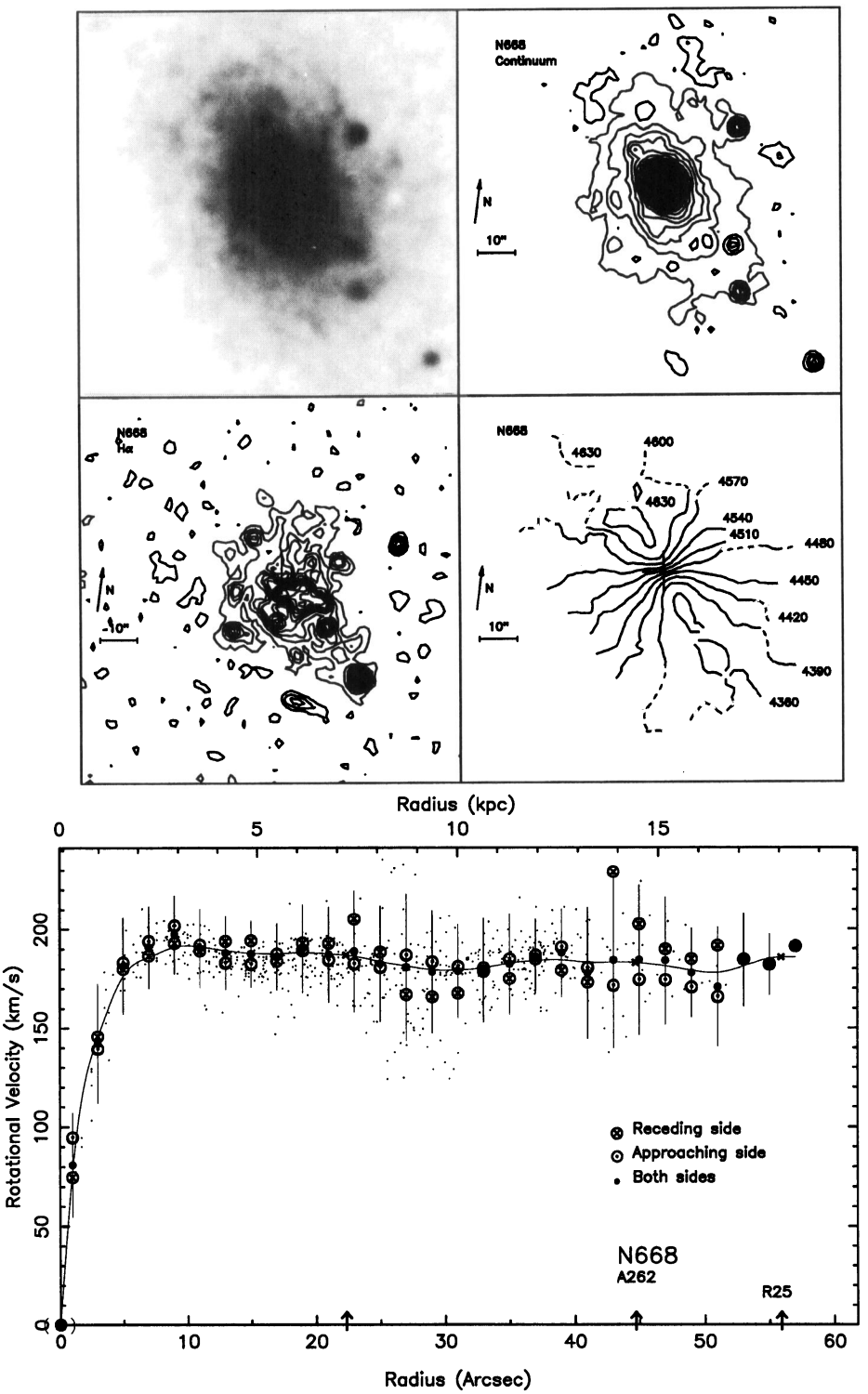

Fig. 1. For each of the 15 galaxies we give the following five figures on a single page: • A photograph: Palomar Sky Survey red print except for NGC 6050/I 1179 (copy of Arp's atlas). • The continuum image near Hα derived from our observations; the contour levels are linearly spaced and of arbitrary value. • The monochromatic Hα image; contour levels are again linearly spaced and of arbitrary value. • Isovelocity contours drawn from the measured values of the heliocentric radial velocity. Dashed lines indicate interpolated values. • Rotation curve derived from the velocity field. The cloud of points represent only that portion of measured velocities within $\pm 30°$ of the major axis in the sky plane. The large velocity points are weighted averages for the entire data set over concentric annuli in the plane of the galaxy. For each annulus we give the average velocity for the receding side ($\otimes$), the approaching side ($\odot$), and the average for both sides (filled circle), the last with a ± 1 rms error bar (in the mean). Points between parentheses are derived from only one or two measured velocities. The curve drawn is a spline function fit to the average values. For the two galaxies already observed by Rubin et al. (1988) with a slit spectrograph, we have also plotted the points of their rotation curve (large squares of arbitrary size) corrected to our inclination. A value of $H_0 = 75$ km s^{-1} Mpc^{-1} has been adopted for the distance scale. The arrows on the horizontal axis indicate the 0.4 R_{25}, 0.8 R_{25}, R_{25} and 1.2 R_{25} values that can be used to calculate various gradients along the rotation curve, small crosses are plotted on the rotation curve at these abscissae. R_{25} is the corrected radius at the 25th magnitude arcsec^{-2} isophote, as given in Table 2

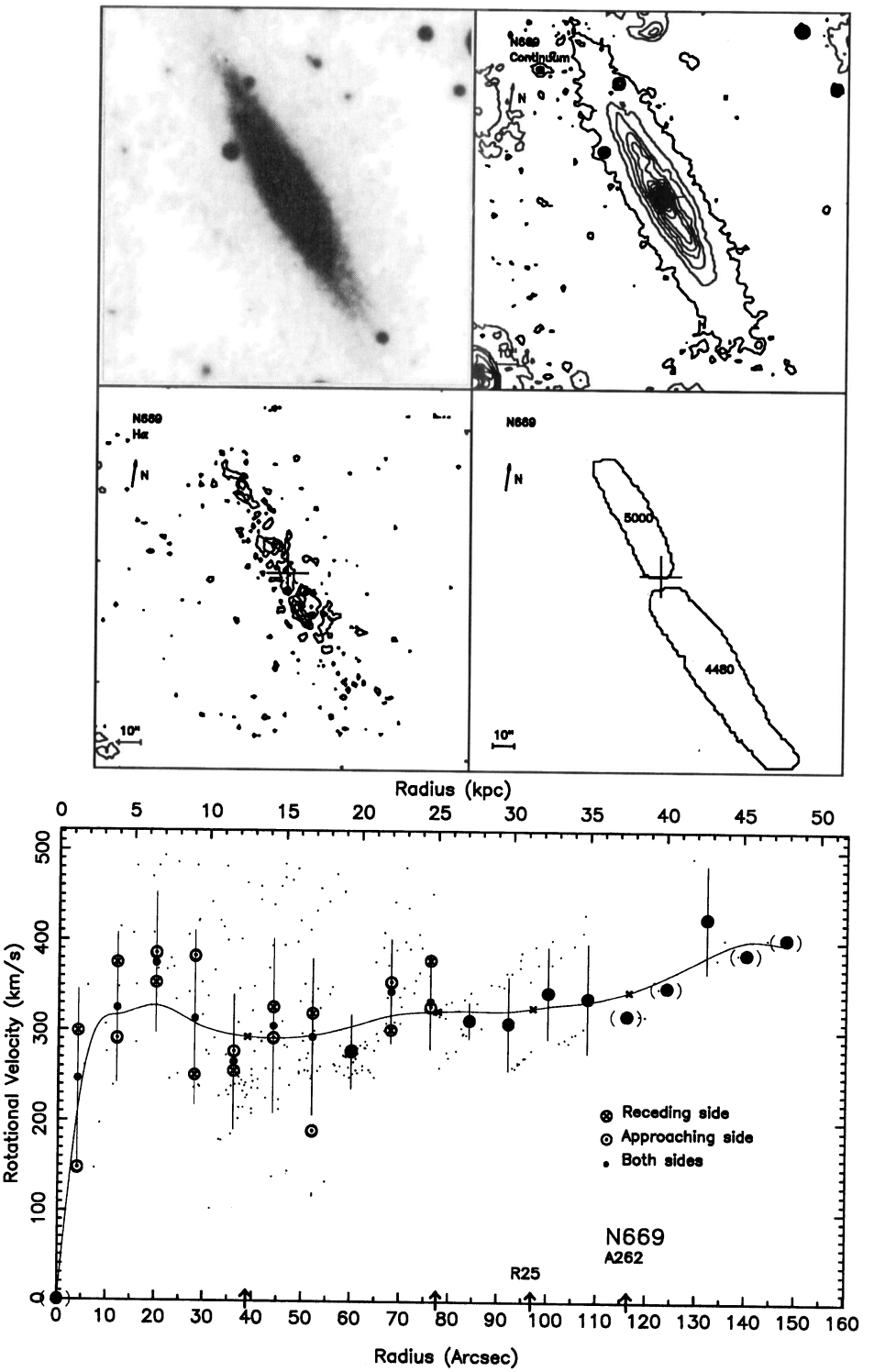

Fig. 1. continued

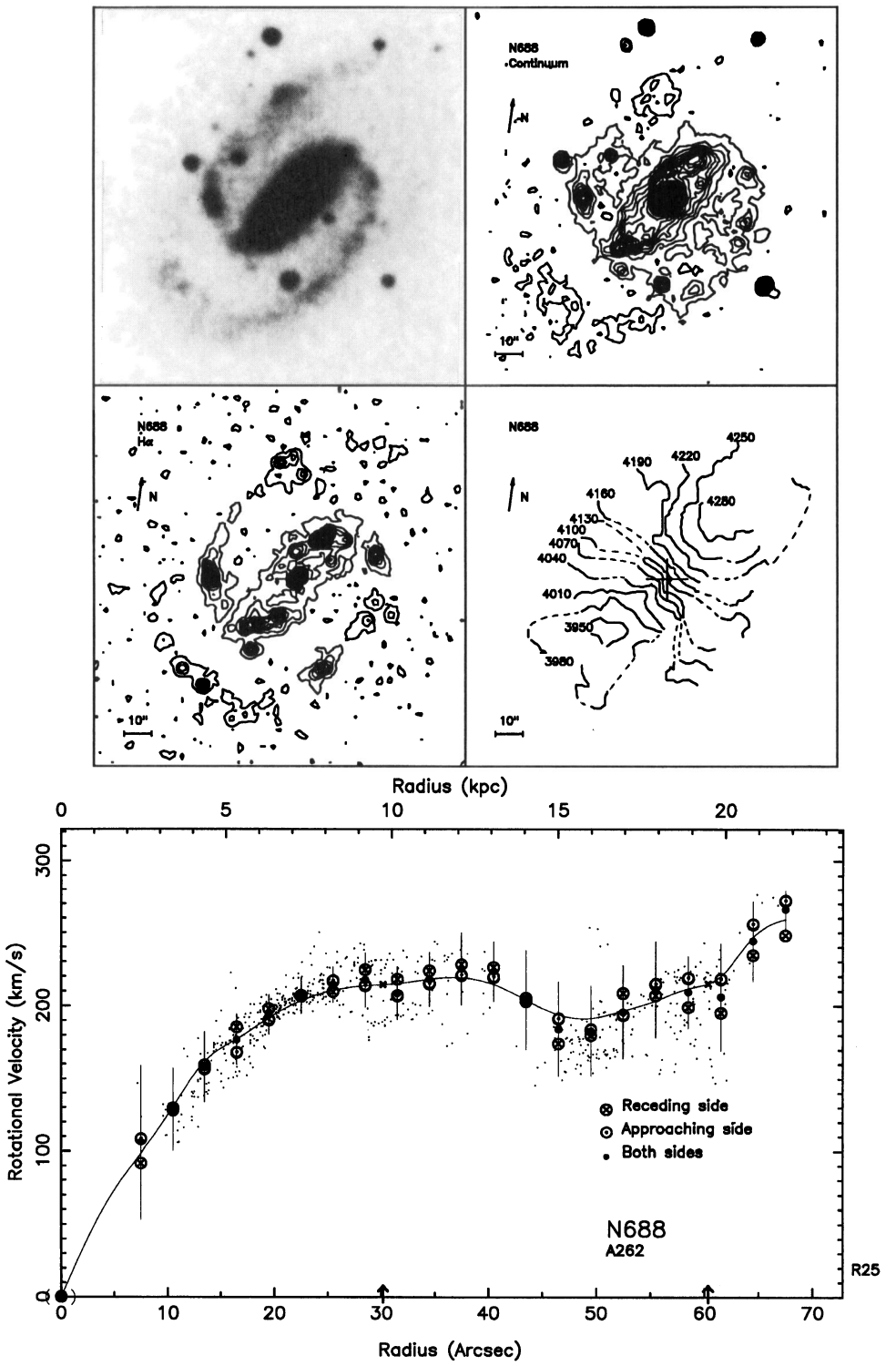

Fig. 1. continued

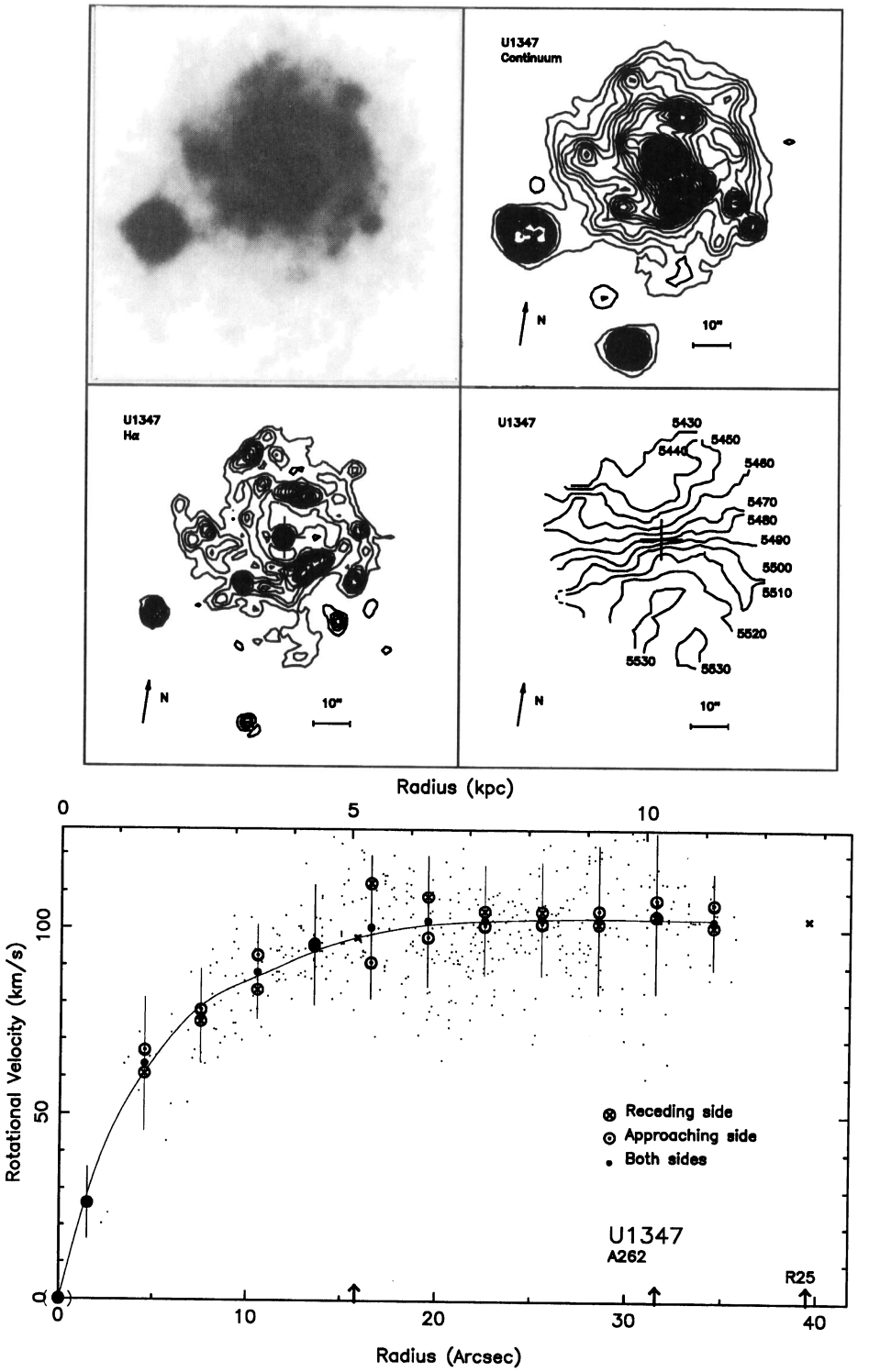

Fig. 1. continued

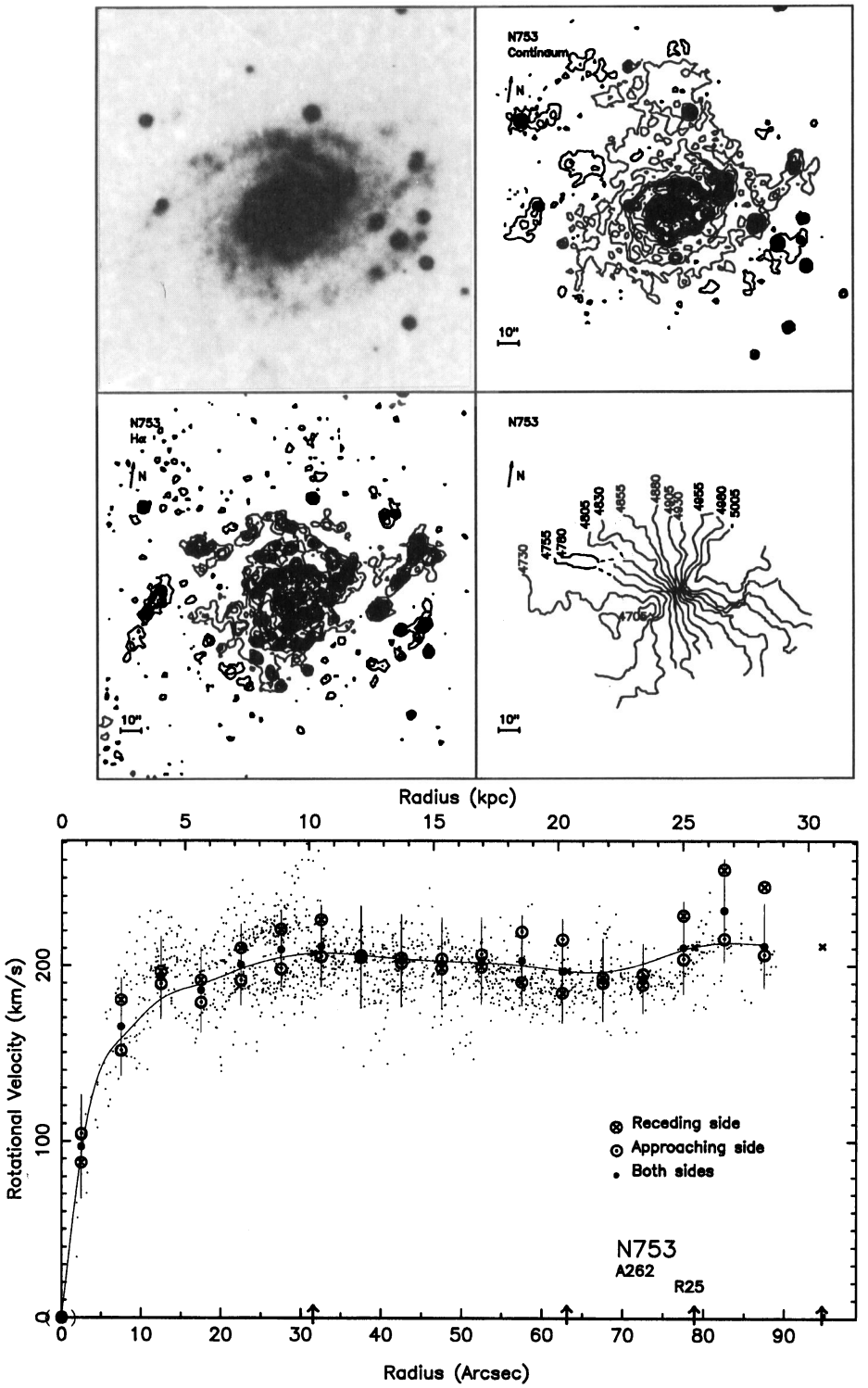

Fig. 1. continued

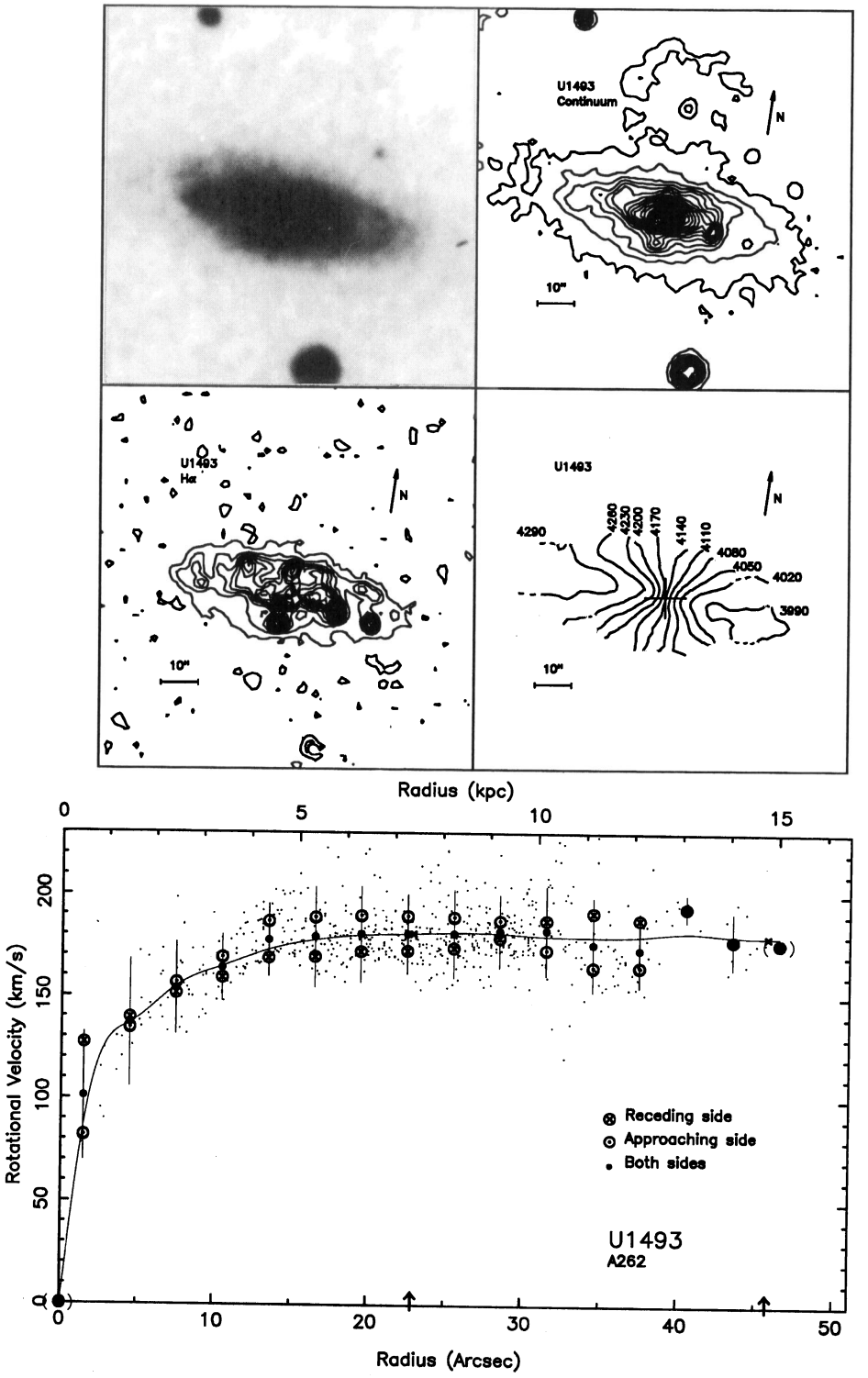

Fig. 1. continued

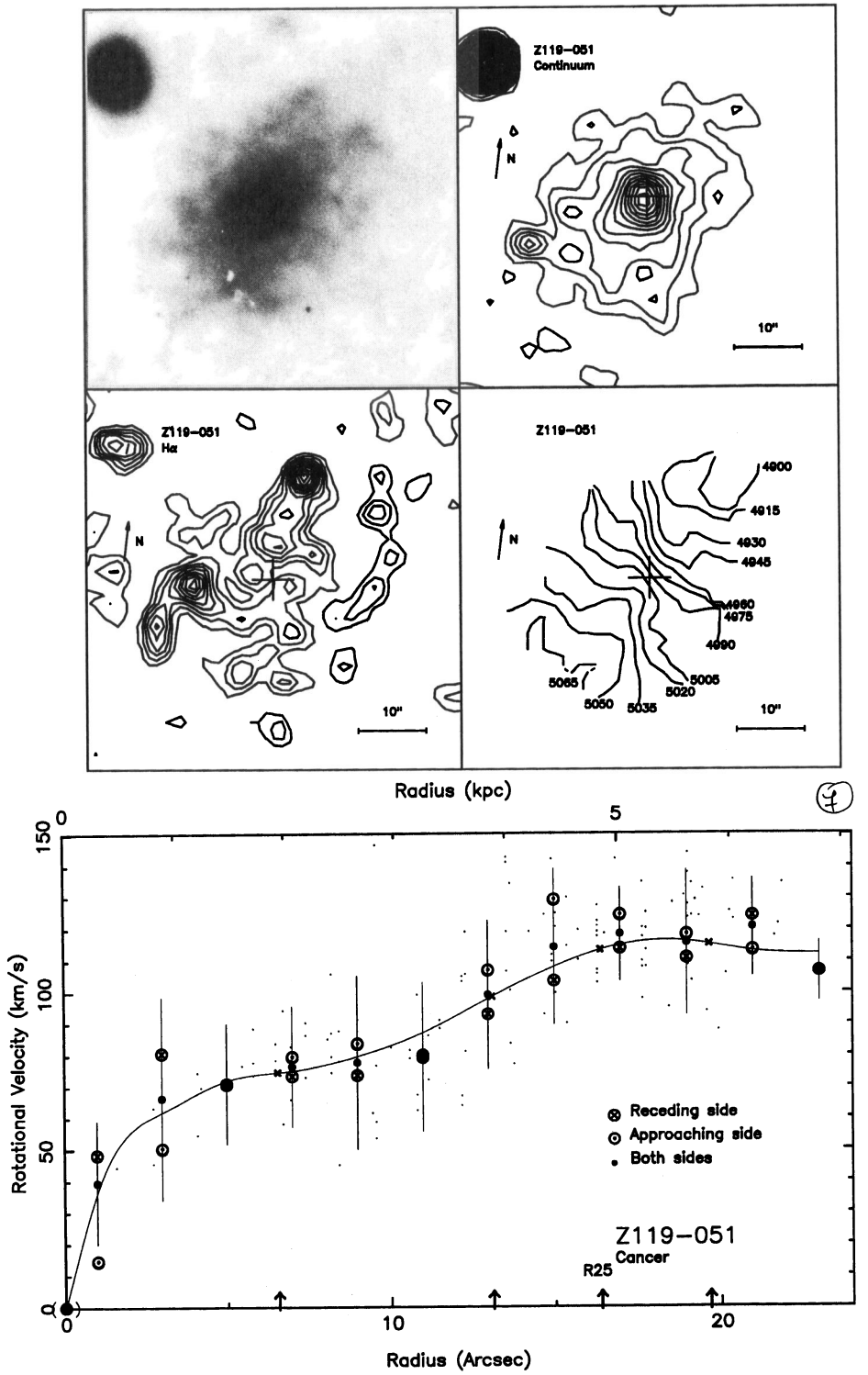

Fig. 1. continued

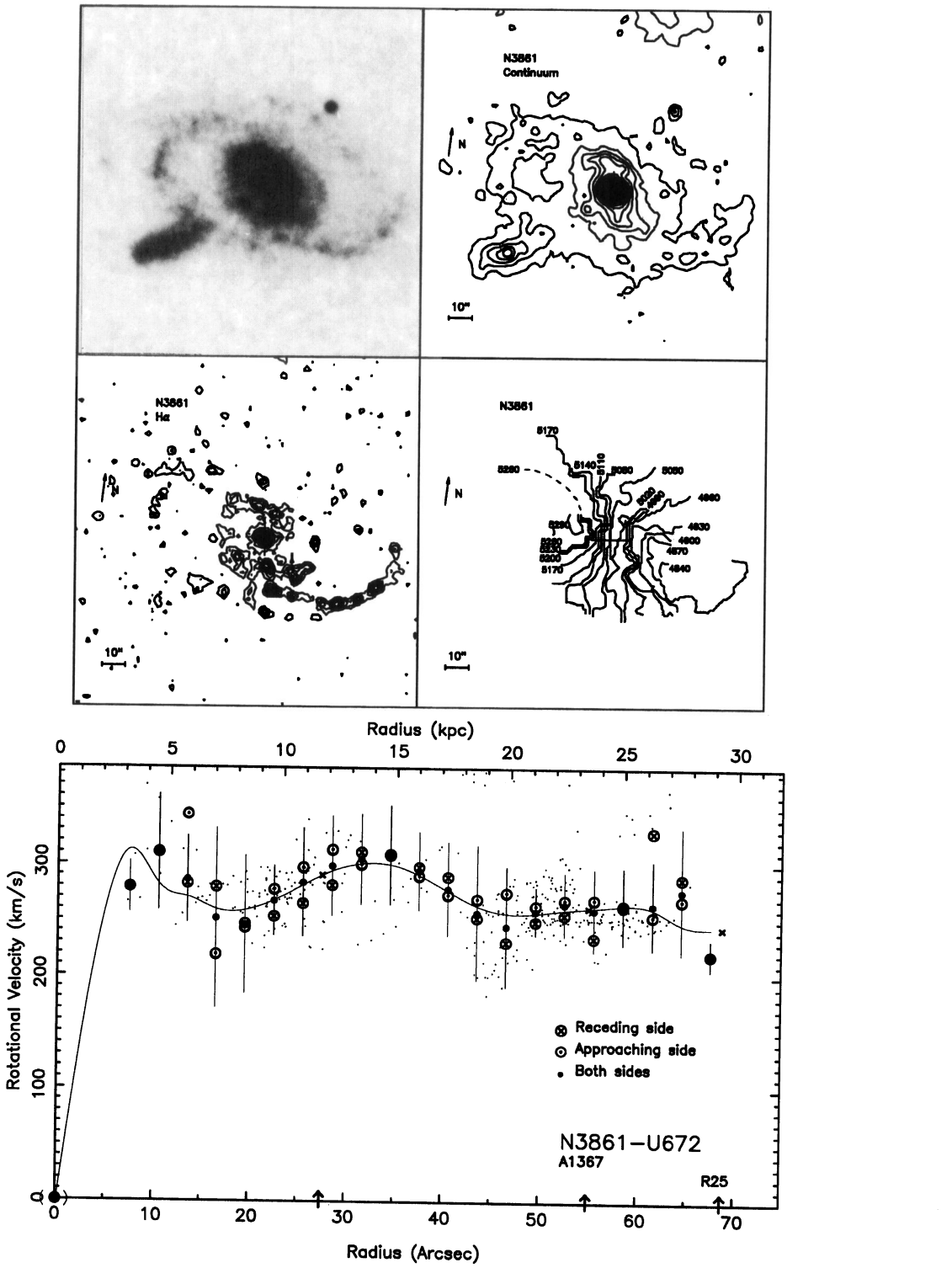

Fig. 1. continued

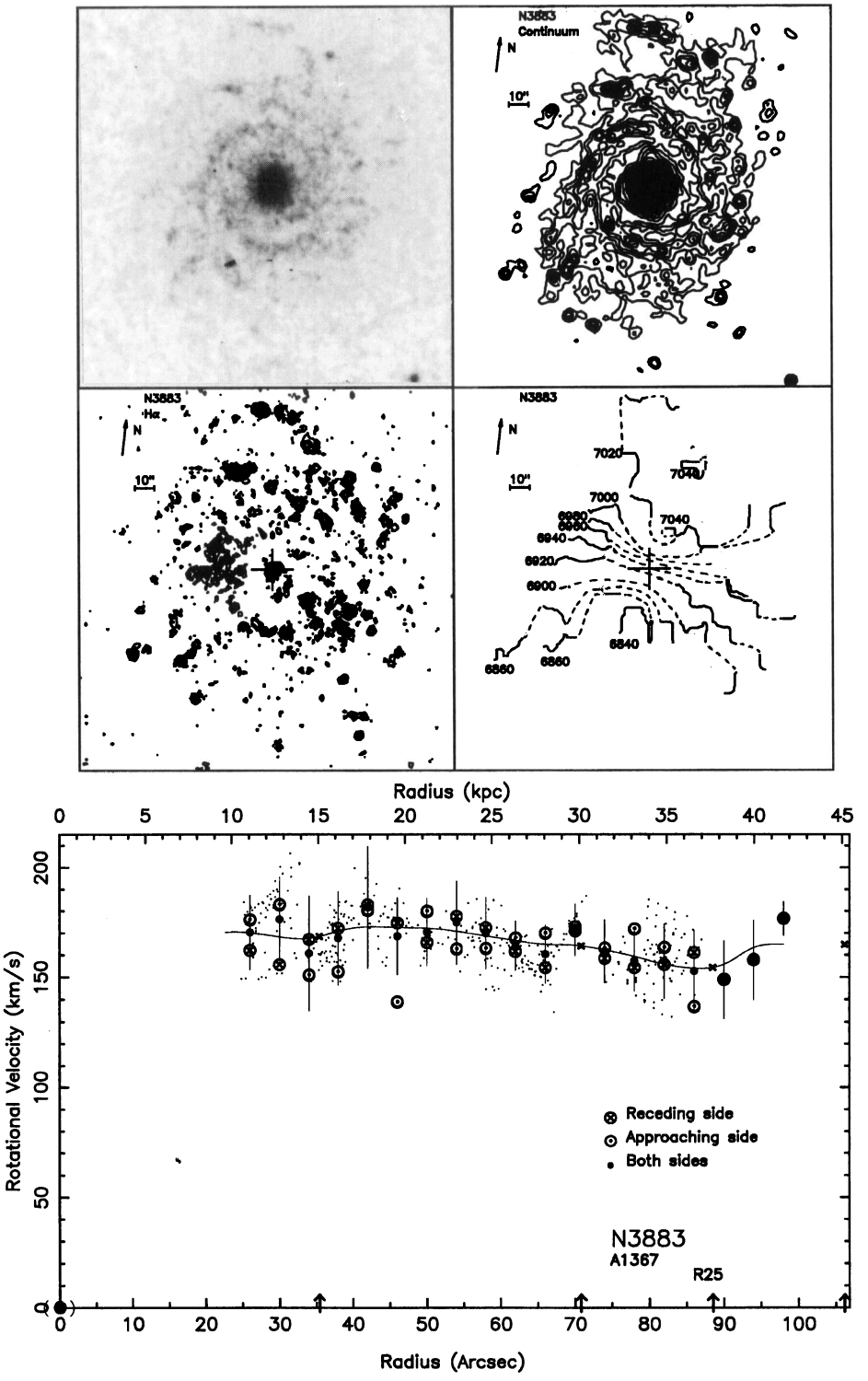

Fig. 1. continued

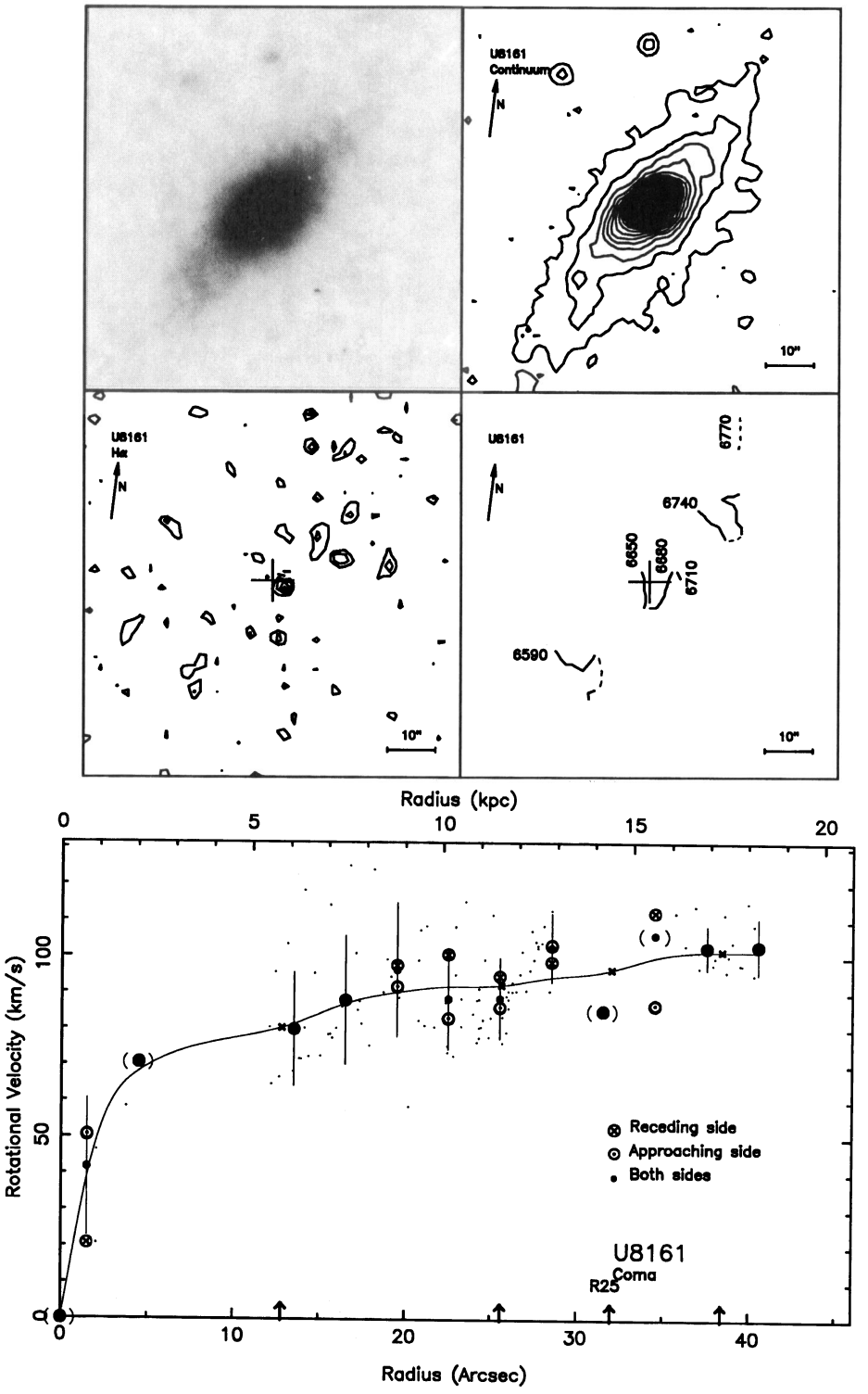

Fig. 1. continued

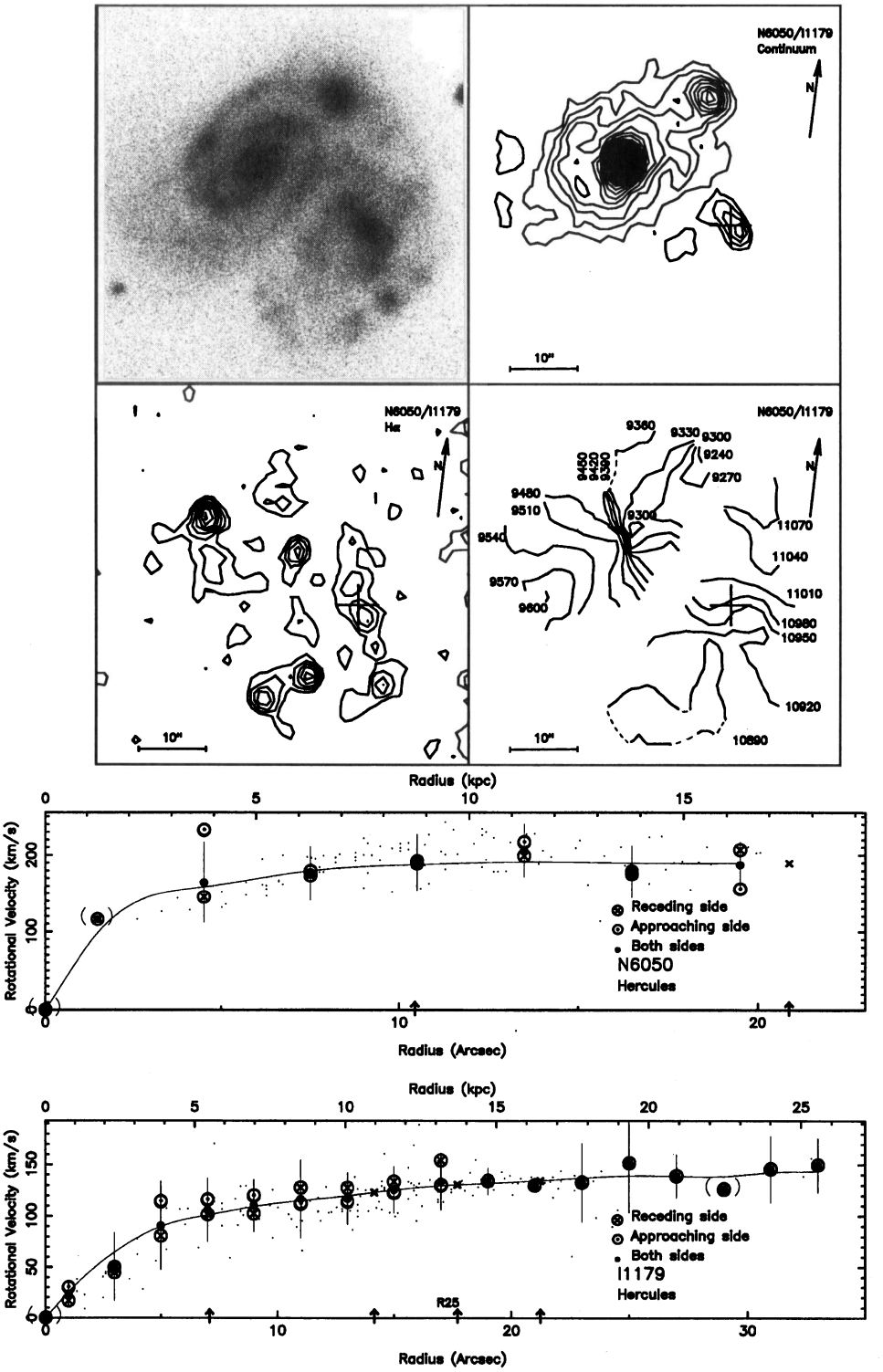

Fig. 1. continued

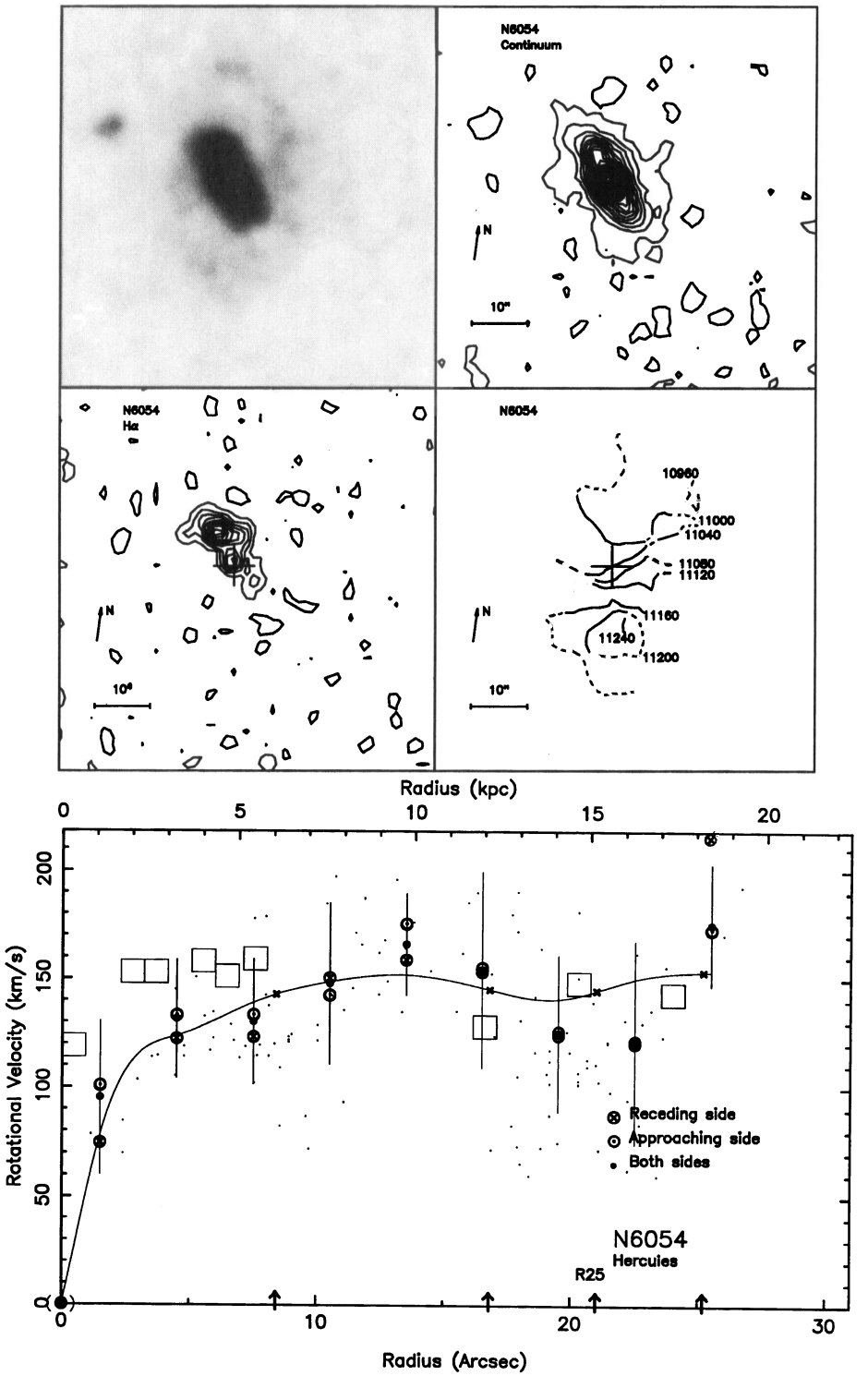

Fig. 1. continued

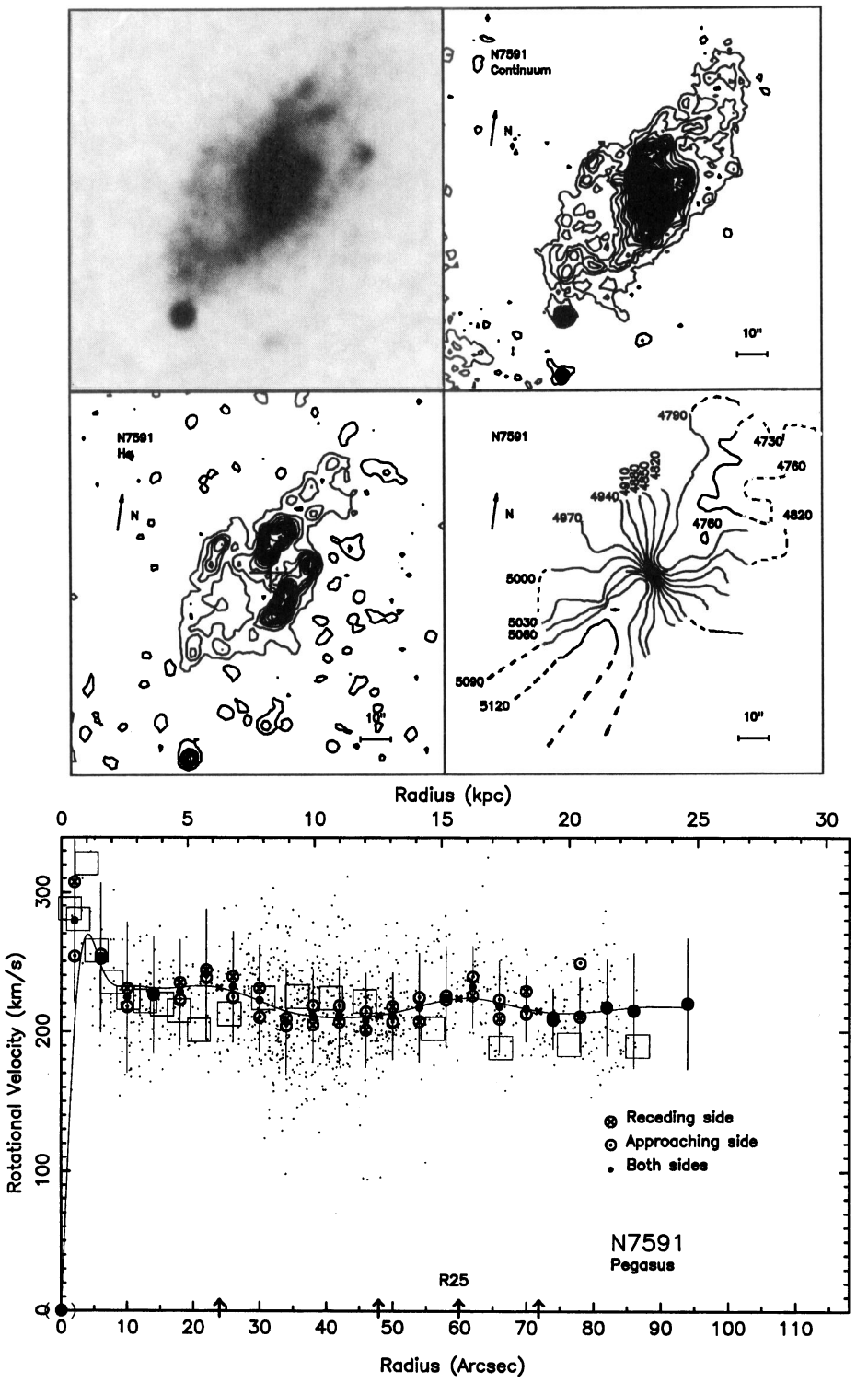

Fig. 1. continued

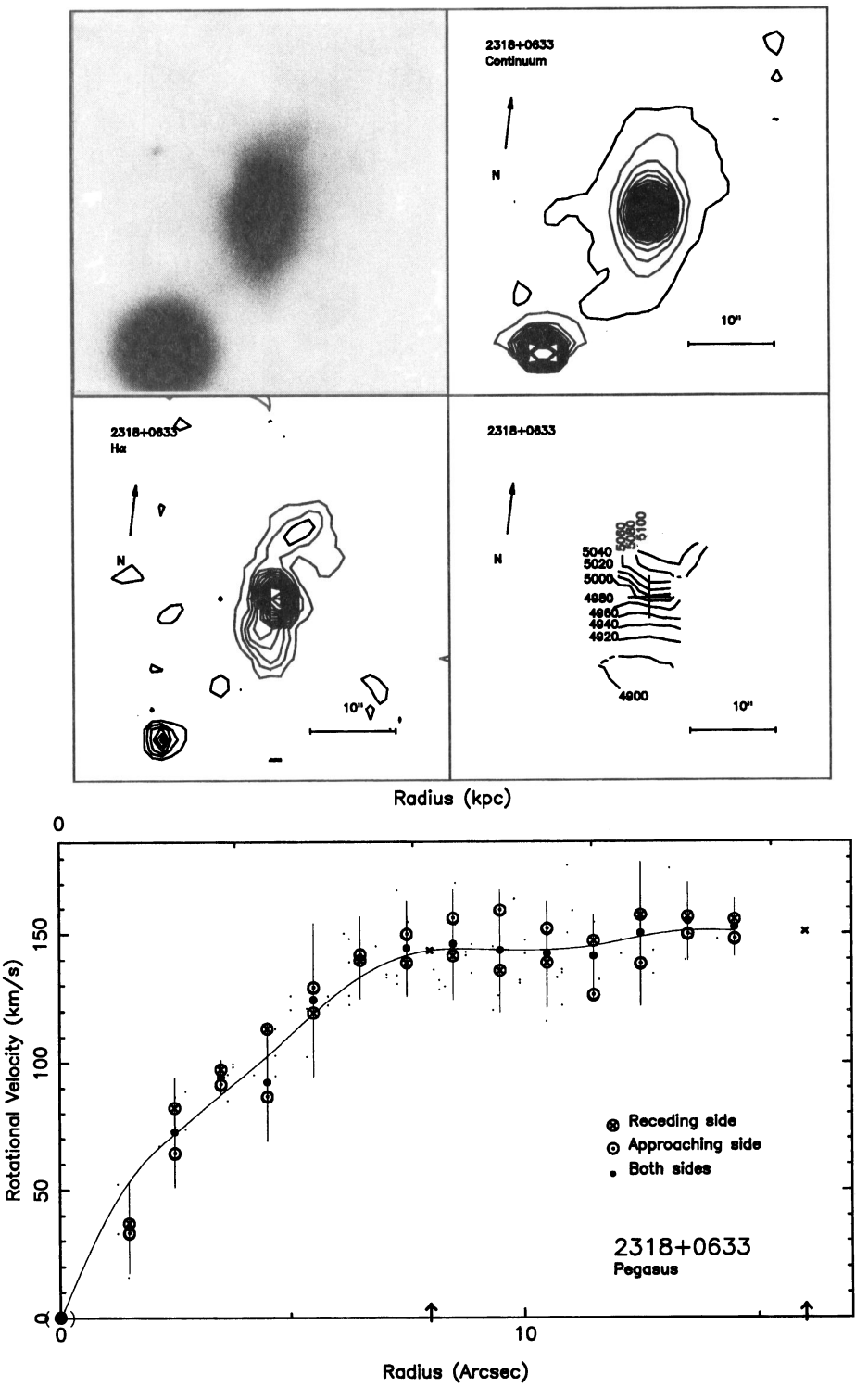

Fig. 1. continued